

# THE TEMPERATURE DIAGNOSTIC PROPERTIES OF THE MG I 457.1 NM LINE

ØYSTEIN LANGANGEN AND MATS CARLSSON<sup>1</sup>

Institute of Theoretical Astrophysics, University of Oslo, P.O. Box 1029 Blindern, N-0315 Oslo, Norway  
*Draft version November 21, 2018*

## ABSTRACT

We analyze the important formation processes for the Mg I 457.1 nm line. This line is an intercombination line and the source function is close to the local thermodynamic equilibrium (LTE) value. The strong coupling to the local temperature and the relatively high population of the lower level (the ground state of Mg I) makes this line an ideal candidate for temperature diagnostics in the lower chromosphere/temperature minimum region. Linking the temperature probed to an absolute physical height is non trivial because of Non-LTE ionization. We analyze the Non-LTE effects and find that photo-ionization from the lower energy levels together with cascading collisional recombination dominate the ionization balance. Taking properly into account the line-blanketing in the UV is essential for obtaining the right photoionization rates. The identification of the main Non-LTE effects in the line allows us to construct a “quintessential” model atom, ideal for computationally demanding tasks, e.g. full 3D and/or time-dependent radiative transfer. Furthermore we analyze the diagnostic potential to temperature of this line in solar-like atmospheres, by synthesizing the line from a series of parametrized atmospheric models. These models have been constructed with fixed effective temperature, but with a variable heat term in the energy equation to obtain a chromospheric temperature rise at different heights. We conclude that the line has a significant potential in the diagnostics of the lower chromosphere temperature structure, especially for cooler atmospheres, such as sunspots.

*Subject headings:* Sun: chromosphere – sunspots

## 1. INTRODUCTION

Deriving the solar atmospheric temperature structure from the emergent spectrum is a classical problem (e.g. Gingerich et al. 1971; Vernazza et al. 1981; Maltby et al. 1986; Fontenla et al. 1993). It became clear quite early that the 1D semi-empirical models would need an increasing temperature in the chromosphere, to explain the increasing radiation temperature with increasing opacity in lines (Athay & Thomas 1961). The existence of such a static temperature rise in the real sun has, however, been questioned (Carlsson & Stein 1995). Hence, it is of great importance to have a good temperature diagnostic for the lower solar chromosphere.

One such candidate is the Mg I 457.1 nm line (from now on the 457.1 line). Note that we here use the common practice in astronomy to use the wavelength in air for naming lines, in vacuum the wavelength is 457.2 nm. The 457.1 line arises from the forbidden transition  $2p^6 3s^2 {}^1S \leftrightarrow 2p^6 3s 3p {}^3P^o$ , hence the source function should be tightly coupled to the local temperature (e.g. Athay & House 1962; Altrock & Canfield 1974; Heasley & Allen 1980; Mauas et al. 1988) due to the dominance of collisions in forbidden lines. The fact that the source function is highly coupled to the local temperature makes the 457.1 line ideal as a diagnostic of the temperature at the height of formation of the line. Early attempts to use this line as a temperature diagnostic include the work of White et al. (1972); Altrock & Cannon (1972); Altrock (1974); Rutten (1977); Heasley & Allen (1980); Mauas et al. (1988). The most important result from this work is that the 457.1 line is formed at around

500 km height in typical quiet sun 1D semi-empirical models, and hence the line will probe the temperature minimum region. Furthermore, the 457.1 line has also been used as a temperature diagnostic for cooler models such as sunspot models (Lites et al. 1987). The modelling often gives a non-observed central reversal in the line core leading to the conclusion that the chromospheric temperature rise must be at a higher position. This result has, however, been questioned (Mauas et al. 1988) due to possible uncertainties in the atomic model. More comprehensive Mg I model atoms have been published like the 66-level atom of Carlsson et al. (1992) and the 83 level atom of Zhao et al. (1998). The 457.1 line has also been used to derive the temperature structure in solar features such as magnetic elements (Briand & Solanki 1995) and flares (e.g. Metcalf et al. 1990a,b).

In this paper we present analysis and results of the temperature diagnostic properties of the 457.1 line. In §2 we analyze the important formation processes of the 457.1 line. As a result of this work we present a minimal realistic model atom (a quintessential model atom) for the 457.1 line in §3. In §4 we parametrize the model atmospheres by solving the radiation hydrodynamics equations with a prescribed heating per unit volume. The atmospheres are allowed to relax and the resulting atmospheres are used to solve the Non-LTE problem for the 457.1 line. Finally we summarize our results in §5.

## 2. FORMATION PROCESSES FOR THE 457.1 LINE

To understand the important formation processes for the 457.1 line we perform and analyse 1D radiative transfer calculations.

### 2.1. Atmospheric models

Electronic address: oysteol@astro.uio.no

<sup>1</sup> also at Center of Mathematics for Applications, University of Oslo, P.O. Box 1053 Blindern, N-0316 Oslo, Norway



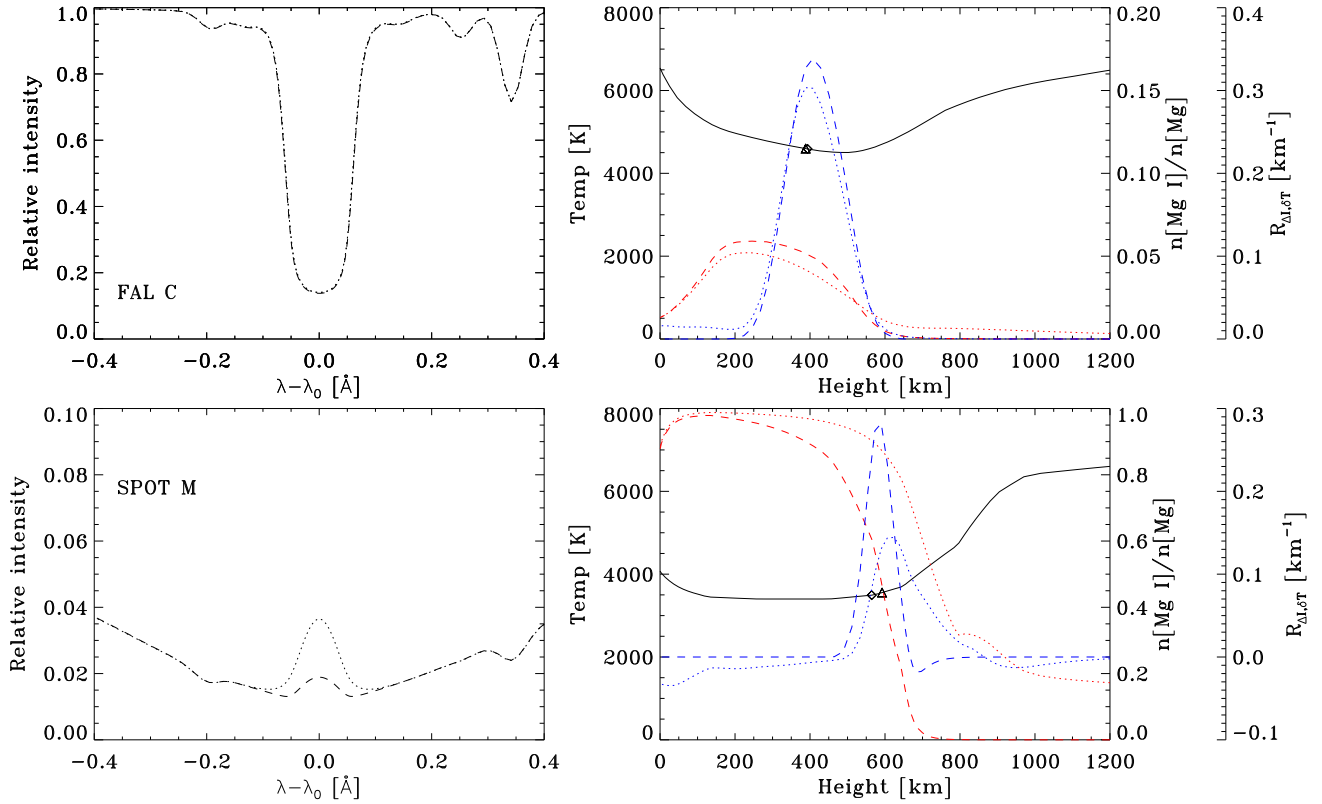


FIG. 2.— FAL C (upper panels) and Spot M (lower panels). Left panels: Emergent profiles in LTE (dashed) and NLTE (dotted). Right panels: temperature (black solid) intensity response functions to temperature calculated in LTE (blue dashed) and NLTE (blue dotted), and neutral fraction in LTE (red dashed) and NLTE (red dotted). The diamonds show where  $\tau_\nu=1$  in LTE and the triangles show similar results in the NLTE case. Note the difference in the Y-axis for the intensity, neutral fraction and response functions between the two atmospheres. Relative intensity is relative to FAL C continuum intensity in both cases.

extent cancel the over-ionization at lower heights in the atmosphere. We investigate these NLTE effect by comparing the rates into the Mg II level from each Mg I level, see Fig.3. As indicated by Fig.3, the dominating effects in the ionization balance of magnesium is radiative ionization from the lower levels, (which dominate because of their relatively high population) especially the Mg I  $2p^6 3s3p\ ^1P^o$  level (level number 3), which has significantly larger photo-ionization crosssection compared to other similar levels. Furthermore, the high energy triplet energy levels play an important role in the ionization balance through collisional recombination (Carlsson et al. 1992; Shimanskaya et al. 2000).

### 2.3.1. Testing the sensitivity of the ionization fraction

To further test the dominating processes in the ionization balance of magnesium, we perform a series of test runs with different degree of realism in the radiative transfer. We test the two main NLTE effects, namely the photoionization and the collisional recombination. For the first effect we run our model atoms with and without taking into account the “UV line haze”. For the second effect, we construct a model atom which does not contain the recombination ladder, essential for the cascading recombination. This is done simply by removing all energy levels, except the Mg II level, with energy above 6.5 eV, see Fig.1 right panel for details on the resulting 11 level atom. The 11 level model atom is quite similar to the older models of the Mg I atom. The results of these tests for the FAL C and the Spot M atmospheres

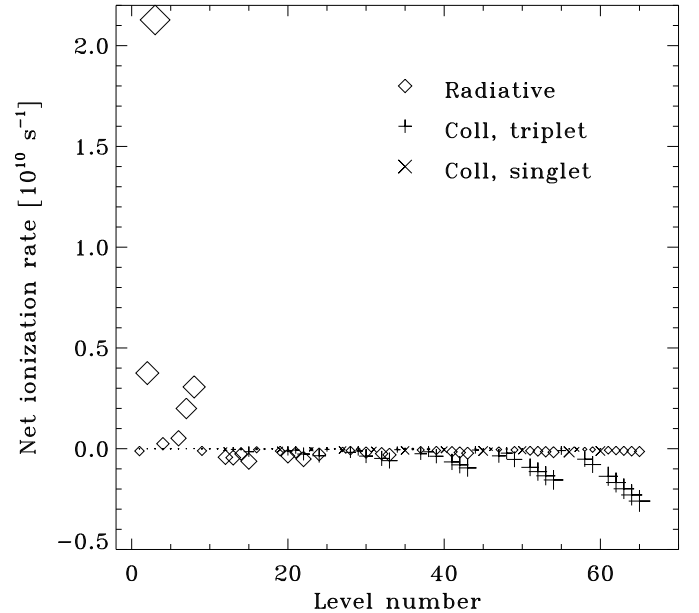


FIG. 3.— Net ionization rates into Mg II from the different levels of Mg I at  $\tau_\nu = 1$  in the FAL C model. The symbol size is scaled to be proportional to the rate. Radiative rates (diamonds), collisions from singlet levels (crosses) and triplet levels (pluses).

are seen in Fig.4 and can be summarized as follows: The largest effect comes from neglecting line blocking with

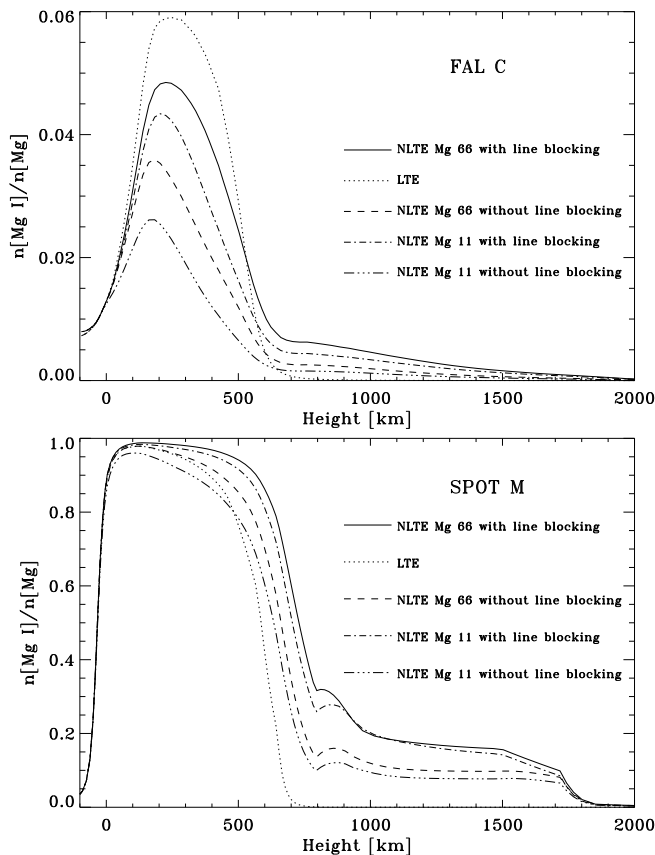


FIG. 4.— neutral fraction in the FAL C (*upper panel*) and Spot M (*lower panel*) models with different level of detail included in the radiative transfer calculations. Note the difference in scaling on the Y-axis between the two panels. Line styles are defined in the figure.

a similar, but slightly smaller, change in the results if the cascading recombination is neglected. It is clear that the NLTE effects are significant, and it is very important that they are included in a realistic manner. If the NLTE effects are included, but with a lacking realism, the deviations from LTE are generally amplified. Finally, to understand the under-ionization high in the atmosphere, and the over-ionization in the lower atmosphere we turn our attention to the radiation field. If  $J_\nu$  is bigger than  $S_\nu$  we have more photons absorbed than emitted and vice versa. Investigating the radiation field for the most important bound-free transition, we see that  $J_\nu$  is larger than  $S_\nu$  where we have over-ionization and smaller than  $S_\nu$  higher in the atmosphere where we have under-ionization.

#### 2.4. Formation processes in the Spot M atmosphere

Similar to the FAL C model we solve the equations of radiative transfer for the Spot M model. The resulting line profiles, LTE and NLTE, are seen in the lower left panel of Fig.2. The difference between the two profiles is significant, especially compared to the similar FAL C profiles. The NLTE solution shows a pronounced increase in the central reversal in the line center of the line. This is basically caused by the higher geometric position of the monochromatic optical depth in NLTE, where the temperature is higher compared to the temperature at the height of formation in LTE. The  $R_{\Delta I, \delta T}$

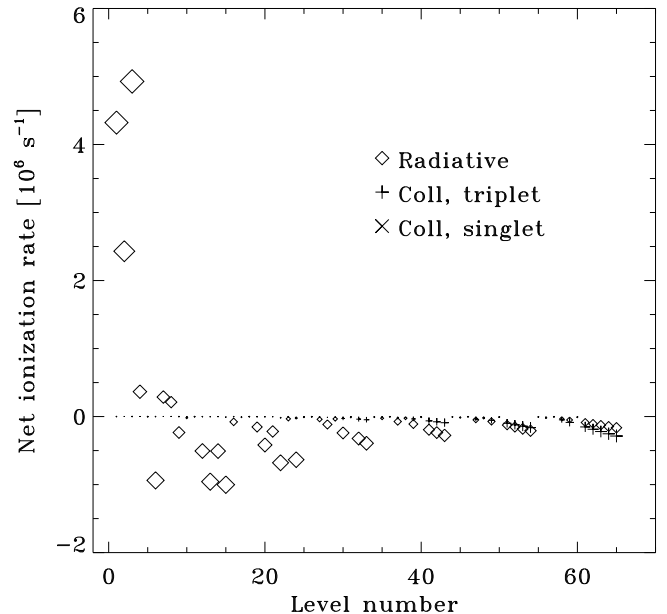


FIG. 5.— Net ionization rates into Mg II from the different levels of Mg I at  $\tau_\nu = 1$  in the 457.1 line in the Spot M model atmosphere. The symbols are scaled to be proportional to the rate. Radiative rates (*diamonds*), collisions from singlet levels (*crosses*) and triplet levels (*pluses*) are plotted.

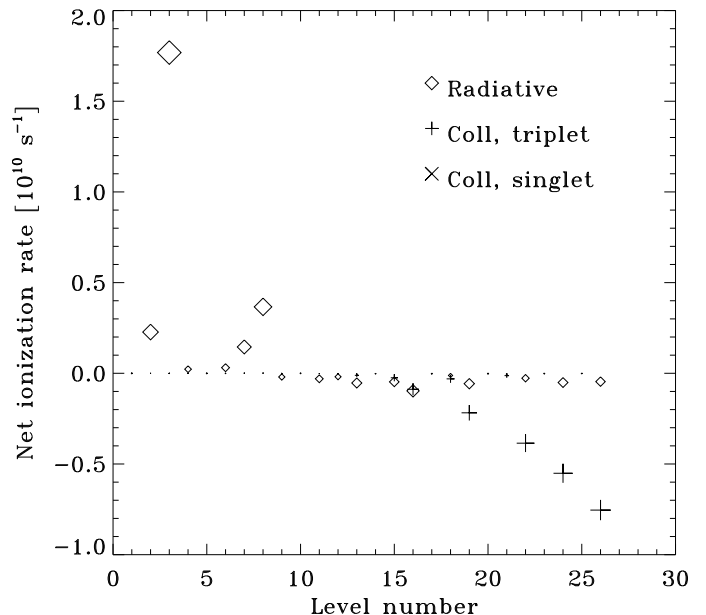


FIG. 6.— Net ionization rates into Mg II from the different levels of Mg I at  $\tau_\nu = 1$  in the 457.1 line using the quintessential 27 level mg atom in the FAL C model atmosphere. The symbols are scaled to be proportional to the rate. Radiative rates (*diamonds*), collisions from singlet levels (*crosses*) and triplet levels (*pluses*) are plotted. Compare to Fig.3.

is much wider in NLTE compared to the LTE case. Furthermore, the  $R_{\Delta I, \delta T}$  has contributions in NLTE from high regions where the temperature has a significant increase. The reason for the increasing formation height in the Spot M model is an increase in the fraction of neutral Mg, see Fig.2 lower right panel. To understand this deviation in ionization fraction, we plot the net rates into the Mg II levels, see Fig.5. As for the FAL C model, we get

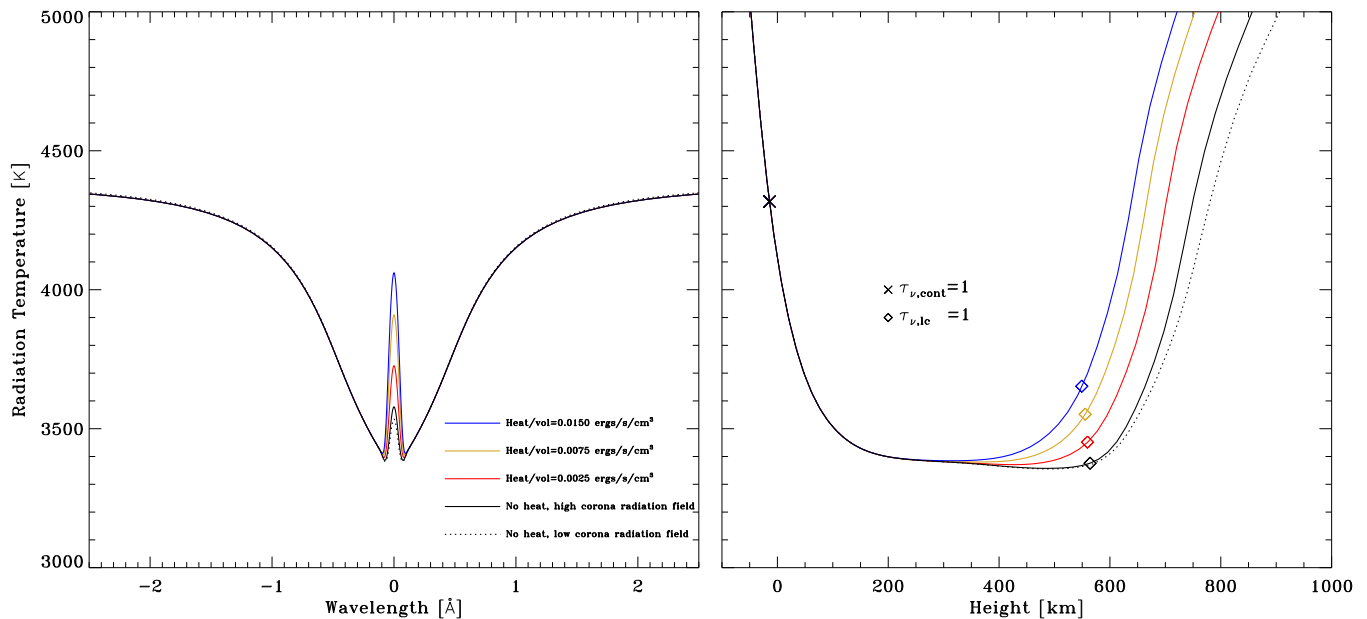


FIG. 7.— Emergent profiles for the different model atmospheres are plotted (*left panel*). The temperature structure of these models is shown (*right panel*). Line styles are showing the different atmospheric models and the corresponding emergent profile. The atmospheres are denoted by the logarithm of the column mass (in cgs units,  $\text{g cm}^{-2}$ ) of the chromospheric temperature increase.

big contributions from the lower levels of the atom, but also the higher excited levels contribute significantly to the ionization fraction, but with a negative contribution. This, together with the cascading collisional recombination, gives much lower ionization fraction for the Mg I atom in the Spot M model. From Fig.4 lower panel, one can see that the ionization fraction is less sensitive to the number of levels in the atom, but much more so for the treatment of line blocking. This is due to the reduced relative importance of the cascading recombination, compared to radiative transitions, see Fig.5

### 3. QUINTESSENTIAL MODEL ATOM

From the above analysis in §2 we have identified the dominating processes in the formation of the 457.1 line. It is then a reasonable question if it is possible to construct a “quintessential” model atom (the smallest atom which reproduces the important physical processes) for this line. Since it is very important to get the ionization fraction correctly for this line, such a quintessential atom must contain a recombination ladder, which satisfactorily mimics the cascading recombination seen in the 66 level model atom.

Following the general procedures outlined by Bard & Carlsson (2008), we construct a quintessential 457.1 line model atom. First, we remove all singlet levels with energy levels above 6.5 eV. This is justified by the small contribution to the overall ionization fraction from these levels, as seen in Fig.3 and in Fig.5. If two levels have a difference in effective quantum number  $\Delta q \leq 0.2$  and at the same time are almost Boltzmann populated ( $\Delta\beta \leq 0.1$ ) in both in the FAL C model and in the Spot M model they are merged. The new model atom is tested in the two atmospheric models, and only accepted if the maximum relative deviation in the emergent intensity (compared to the full atom) is less than 25%. This procedure is repeated until all levels have been tested. The resulting model atom is reduced

to a 27 level atom; see Fig.1, which is a reduction to less than half the size of the original atom.

Further reduction is possible, but only with more liberal acceptance conditions, which would affect the realism of the model atom. The new model atom mimics the recombination ladder in the full model atom, by super levels as seen in Fig.6 and Fig.3.

The quintessential model atom was also tested against the original atom using a series of dynamic atmospheres taken from Carlsson & Stein (1997). This test gives a deviation between the lineprofiles of less than 3% between the two models atoms, and deviations in the bisector Doppler shifts of usually less than  $10 \text{ m s}^{-1}$  and always less than  $30 \text{ m s}^{-1}$ .

### 4. PARAMETRIZATION OF THE TEMPERATURE DIAGNOSTICS

In the above analysis we have seen that the 457.1 line shows a strong central reversal in a cool sunspot atmosphere, but in a hotter quiet sun model there is no such reversal. The reason for the lack of reversal in the hotter model is the high ionization fraction in such models, which deplete the number densities of the lower level in the 457.1 line and put the formation height below the chromospheric temperature rise. From here on we focus on cool sunspot models, since the 457.1 line has a clear diagnostic potential for such models. We are especially interested in the possible bound the central reversal put on the position of the temperature rise in such models.

To investigate the diagnostic properties of the line further, we construct a series of 1D self consistent radiative hydrodynamics model atmospheres. We use the radyn code (Carlsson & Stein 1992, 1995, 1997, 2002), to construct these model atmospheres. In short this code solves the mass, momentum, and energy conservation equations together with the detailed equations of radiative transfer for three of the important elements in the energy balance (H, Ca, and He) on an adaptive grid

(Dorfi & Drury 1987). The boundary condition in the deep photospheric part (column mass  $\geq 15 \text{ g cm}^{-2}$ ) of the atmosphere is taken from a 4000 K effective temperature model without convection generated by the MARCS code (Gustafsson et al. 2008). The temperature structure in these deep parts of the atmosphere is fixed by adding a new term to energy equation in this region.

The incoming UV radiation field from the corona has to be specified at the upper boundary. To facilitate such a boundary condition we use the data of Tobiska (1991) and follow the method used by Wahlstrom & Carlsson (1994). Since the model used by Wahlstrom & Carlsson (1994) was based on a quiet sun corona, we expect that this model underestimate the coronal radiation field. We have performed tests (a more thorough analysis of this effect will be given in an upcoming paper) with different scaling of the incoming radiation field, and found that the radiation field has profound effects on the chromospheric temperature structure. From these tests we conclude that the incoming radiation field should be scaled up by at least a factor 5. With the above described boundary conditions, we allow the atmospheres to converge to an equilibrium state, and the pressure at the top of the simulations is changed until there are no more outflowing material. The resulting temperature structures for an active and a quiet corona are seen in Fig.7 right panel. The difference in the chromospheric temperature structure due to scaling of the coronal radiation field is quite big, however the effect on the 457.1 line is rather small due to the low formation height, see Fig.7 left panel. For the construction of the atmospheres used in this analysis we adopt a scaling factor of 5 for the coronal radiation field.

We parametrize the position of the chromospheric temperature increase in the theoretical model atmosphere by adding a constant heat term in the energy equation. To avoid unrealistic temperature structures in the lower part of the atmosphere, the heat term has to be defined per volume and not per mass. The latter will lead to an increase in temperature at very low atmospheric heights (Bard & Carlsson 2004). Since the heating term per volume will lead to a very high energy input in the corona, we allow a smooth transition to heat per mass above the transition region in the original atmosphere. The exact position of this smooth transition is changing the temperature structure in the corona, and to some extent the upper chromosphere, but it has no effect on the emergent 457.1 line profile. Furthermore, the heat term leads to an expanding corona but flows due to this expansion at the formation height of the 457.1 line are very small, typically less than  $10 \text{ ms}^{-1}$  and hence negligible.

We construct different atmospheres by adding different heat terms per volume to the energy equation as described above. In this way we construct a grid of self consistent atmospheres with different position of the chromospheric temperature rise. Note that we use this parametrization of the temperature because it is only dependent on one parameter (the magnitude of the constant heat term added to the energy equation). Furthermore, these models should be considered a parametrization of the position of the chromospheric temperature increase, and *not* a parametrization to evaluate the energy balance in the chromosphere.

Some of the resulting temperature structures are seen in Fig.7 right panel. As seen in the left panel of Fig.7 the emergent 457.1 line profile shows a significant increase in the central reversal with decreasing height of the chromospheric temperature rise. Note that these line profiles have been calculated using the quintessential modelatom and without including the nearby lines (to avoid confusion). The size of the reversal is increased by the increasing temperature at the monochromatic optical depth of the line center of the 457.1 line. Note that the position of the monochromatic optical depth is only slightly changed with the changes in the position of the chromospheric temperature rise. The reason for this rather constant formation height is the high number densities of the Mg I ground state. If the temperature is increased, the relative change in the ionization fraction is changed only slightly due to the high density of Mg I atoms.

Note the inconsistency between the emergent profile and the Eddington-Barbier approximation applied on the temperature structures in Fig.7. The reason for the lacking correspondence is the deviation of the source function/temperature from a linear function in  $\tau_\nu$ . Since the Eddington-Barbier approximation is not very good, it is not very instructive to invert the temperature profile from such assumptions. However, the reversals are strong enough to discriminate between different models. We recommend a forward modeling approach to the temperature diagnostics, similar to the work by Lites et al. (1987). From these theoretical models the 457.1 line can be used to set lower bounds on the position of the chromospheric temperature increase. The sensitivity of such a discrimination will of course depend on the sensitivity of the observations used for the comparison.

## 5. CONCLUSION

We have analysed the dominant NLTE effects of the 457.1 line in two solar models (FAL C and Spot M), and concluded that the ionization from the lower levels, especially the Mg I  $2p^6 3s 3p^1 P^o$ , is the main contribution to the ionization. Furthermore, cascading collisional recombination in the triplet system plays an important role in the NLTE formation processes in the 457.1 line. With the understanding of the formation processes for the 457.1 line, it is possible to construct a “quintessential” model atom. We have presented a 27 level quintessential model atom (an atom with the minimum number of levels, that maintain the important physical processes).

We have found that increasing the realism in the model atom does not remove the non-observed central reversal in the Spot M model, as claimed by Mauas et al. (1988).

Finally we have presented a series of sunspot models where the height of the chromospheric temperature rise has been varied. These models show that the height of formation of the 457.1 line is not very sensitive to the height of the chromospheric temperature rise but the central reversal is. The amount of emission in the line core is thus a sensitive diagnostic of the lower chromosphere temperature structure and a lack of central reversal puts a strong constraint on the lowest possible position of the chromospheric temperature increase.

*Acknowledgments.* This research was supported by the Research Council of Norway through grant 170935/V30 and a grant of computing time from the Program for Supercomputing. This research has made use of NASA’s

## REFERENCES

- Altrock, R. C. 1974, *Sol. Phys.*, 34, 37
- Altrock, R. C., & Canfield, R. C. 1974, *ApJ*, 194, 733
- Altrock, R. C., & Cannon, C. J. 1972, *Sol. Phys.*, 26, 21
- Asplund, M., Grevesse, N., & Sauval, A. J. 2005, in *Astronomical Society of the Pacific Conference Series*, Vol. 336, *Cosmic Abundances as Records of Stellar Evolution and Nucleosynthesis*, ed. T. G. Barnes, III & F. N. Bash, 25–+
- Athay, R. G., & House, L. L. 1962, *ApJ*, 135, 500
- Athay, R. G., & Thomas, R. N. 1961, *Physics of the solar chromosphere* (Interscience Monographs and Texts in Physics and Astronomy, New York: Interscience Publication, 1961)
- Bard, S., & Carlsson, M. 2004, in *IAU Symposium*, Vol. 223, *Multi-Wavelength Investigations of Solar Activity*, ed. A. V. Stepanov, E. E. Benevolenskaya, & A. G. Kosovichev, 445–446
- Bard, S., & Carlsson, M. 2008, *ApJ*, 682, 1376
- Briand, C., & Solanki, S. K. 1995, *A&A*, 299, 596
- Carlsson, M. 1986, *A Computer Program for Solving Multi-Level Non-LTE Radiative Transfer Problems in Moving or Static Atmospheres* (Uppsala Astronomical Observatory: Report No. 33)
- Carlsson, M., Rutten, R. J., & Shchukina, N. G. 1992, *A&A*, 253, 567
- Carlsson, M., & Stein, R. F. 1992, *ApJ*, 397, L59
- . 1995, *ApJ*, 440, L29
- . 1997, *ApJ*, 481, 500
- . 2002, *ApJ*, 572, 626
- Collet, R., Asplund, M., & Thévenin, F. 2005, *A&A*, 442, 643
- Dorfi, E. A., & Drury, L. O. 1987, *Journal of Computational Physics*, 69, 175
- Fontenla, J. M., Avrett, E. H., & Loeser, R. 1993, *ApJ*, 406, 319
- Fossum, A., & Carlsson, M. 2005, *ApJ*, 625, 556
- Gingerich, O., Noyes, R. W., Kalkofen, W., & Cuny, Y. 1971, *Sol. Phys.*, 18, 347
- Gustafsson, B., Edvardsson, B., Eriksson, K., Jørgensen, U. G., Nordlund, Å., & Plez, B. 2008, *A&A*, 486, 951
- Heasley, J. N., & Allen, M. S. 1980, *ApJ*, 237, 255
- Kupka, F., Piskunov, N., Ryabchikova, T. A., Stempels, H. C., & Weiss, W. W. 1999, *A&AS*, 138, 119
- Lites, B. W., Skumanich, A., Rees, D. E., Murphy, G. A., & Carlsson, M. 1987, *ApJ*, 318, 930
- Magain, P. 1986, *A&A*, 163, 135
- Maltby, P., Avrett, E. H., Carlsson, M., Kjeldseth-Moe, O., Kurucz, R. L., & Loeser, R. 1986, *ApJ*, 306, 284
- Mauas, P. J., Avrett, E. H., & Loeser, R. 1988, *ApJ*, 330, 1008
- Metcalfe, T. R., Canfield, R. C., Avrett, E. H., & Metcalfe, F. T. 1990a, *ApJ*, 350, 463
- Metcalfe, T. R., Canfield, R. C., & Saba, J. L. R. 1990b, *ApJ*, 365, 391
- Piskunov, N. E., Kupka, F., Ryabchikova, T. A., Weiss, W. W., & Jeffery, C. S. 1995, *A&AS*, 112, 525
- Rutten, R. J. 1977, *Sol. Phys.*, 51, 3
- Ryabchikova, T., Piskunov, N., Stempels, H., Kupka, F., & Weiss, W. 1999, *Physica Scripta*, T83, 162
- Shimanskaya, N. N., Mashonkina, L. I., & Sakhibullin, N. A. 2000, *Astronomy Reports*, 44, 530
- Tobiska, W. K. 1991, *Journal of Atmospheric and Terrestrial Physics*, 53, 1005
- Vernazza, J. E., Avrett, E. H., & Loeser, R. 1981, *ApJS*, 45, 635
- Wahlstrom, C., & Carlsson, M. 1994, *ApJ*, 433, 417
- White, O. R., Altrock, R. C., Brault, J. W., & Slaughter, C. D. 1972, *Sol. Phys.*, 23, 18
- Zhao, G., Butler, K., & Gehren, T. 1998, *A&A*, 333, 219